

# Influence of degree of sulfation on the rheology of cellulose nanocrystal suspensions

Sadaf Shafiei-Sabet · Wadood Y. Hamad ·  
Savvas G. Hatzikiriakos

Received: 22 March 2013 / Revised: 8 June 2013 / Accepted: 20 June 2013 / Published online: 6 July 2013  
© Springer-Verlag Berlin Heidelberg 2013

**Abstract** The rheology and microstructure of two different cellulose nanocrystals (CNC) samples possessing different degrees of sulfation are studied over a broad concentration range of 1 to 15 wt%. CNC suspensions are isotropic at low concentration and experience two different transitions as concentration increases. First, they form chiral nematic liquid crystals above a first critical concentration where the samples exhibit a fingerprint texture and the viscosity profile shows a three-region behavior, typical of liquid crystals. By further increasing the concentration, CNC suspensions form gels above a second critical concentration, where the viscosity profile shows a single shear-thinning behavior over the whole range of shear rates investigated. It has been found that the degree of sulfation of CNC particles has a significant effect on the critical concentrations at which transitions from isotropic to liquid crystal and liquid crystal to gel occur. Rheological properties and microstructure of these suspensions have been studied using polarized optical microscopy combined with rheometry.

**Keywords** Cellulose nanocrystals (CNC) · Rheology · Suspension · Sonication · Chiral nematic · Liquid crystal · Degree of sulfation

## Introduction

Strong acid hydrolysis of cellulose fibers, or other ligno-cellulosic raw materials, leads to extraction of highly crystalline cellulose nanoparticles (Marchessault et al. 1961; Revol et al. 1992). These rod-like crystallites are of colloidal dimension and are termed cellulose nanocrystals (CNC) or nanocrystalline cellulose. The hydrolysis conditions affect the size and surface properties of cellulose nanocrystals (Dong et al. 1998). Sulfuric acid hydrolysis results in CNC particles with anionic sulfur groups on the surface, leading to electrostatically stabilized CNC aqueous suspensions (Marchessault et al. 1959, 1961; Revol et al. 1992; Revol and Marchessault 1994; Dong et al. 1996). These suspensions form liquid crystal chiral nematic ordered phases above a critical concentration (Revol et al. 1992) and display the optical characteristics typical of chiral nematic (cholesteric) liquid crystals. This phase separation (i.e., formation of a chiral nematic phase) in CNC aqueous suspensions is generally governed by basic properties of the nanoparticles, namely, physical dimension, size polydispersity, surface charge, and the ionic strength of the system (Onsager 1949; Odijk 1986; Dong et al. 1998; Hamad and Hu 2010).

Due to formation of liquid crystalline ordered domains in these systems, CNC suspensions have a complicated microstructure which controls the macroscopic flow behavior of the material and is sensitive to applied flow fields similar to other systems such as rod-like virus suspensions (Lettinga et al. 2005; Kang et al. 2006; Ripoll et al. 2008; Boluk et al. 2011). Comparing the flow properties in the disordered and ordered states, the transition from isotropic to liquid crystal ordered phases have been characterized (Orts et al. 1998; Bercea and Navard 2000; Shafiei-Sabet et al. 2012). In addition to the isotropic-liquid crystal transition, CNC suspensions experience another transition from liquid

S. Shafiei-Sabet · S. G. Hatzikiriakos (✉)  
Chemical and Biological Engineering, The University of British  
Columbia, Vancouver, British Columbia V6T 1Z3, Canada  
e-mail: savvas.hatzi@ubc.ca

W. Y. Hamad  
FPIInnovations, 3800 Wesbrook Mall, Vancouver, British  
Columbia V6S 2L9, Canada

crystal to gel at a higher critical concentration. This second transition has been reported recently (Liu et al. 2011; Urena-Benavides et al. 2011; Shafiei-Sabet et al. 2012); however, its effect on rheology and the governing factors that control rheological properties have not been explored and need to be systematically investigated.

In this paper, the rheological behavior and microstructure of two different sets of CNC aqueous suspensions, hydrolyzed to produce different degrees of sulfation, are studied over a broad range of concentrations (1 to 15 wt%), and their physicochemical properties were examined. Furthermore, the effect of the degree of sulfation on the critical concentration of two different microstructure transitions, isotropic to liquid crystal and liquid crystal to gel, are studied using rheometry and polarized optical microscopy, for the first time. The applicability of the Cox–Merz rule as a function of concentration and degree of sulfation is also evaluated in order to gain a better understanding of the rheological complexity of these systems.

## Experimental

### CNC extraction and suspension preparation

Two different sets of CNC suspensions, CNC-A and CNC-B, were prepared by hydrolysis of black spruce kraft pulp (BSKP) using 64 % *w/w* sulfuric acid at 45 °C for 25 min according to Hamad and Hu (2010). The preparation conditions for these two sets of CNC suspensions are summarized in Table 1. Post-hydrolysis processing was controllably modified to produce CNC suspensions with different sulfur contents, or degrees of sulfation (see Table 2). To obtain cellulose crystals of colloidal dimensions, the suspensions were sonicated (ultrasonic processor VCX-130, Sonics and Materials Inc.) for 15 min at 60 % max power, while being cooled in an ice bath. Since H-form CNC cannot easily be re-dispersed in water, the suspensions were then titrated with 0.1 M NaOH to replace the hydrogen ions on the surface of the CNC particles with sodium ions; this step is necessary to ensure that the suspension has reached the right pH (~7). The suspensions were then freeze-dried, and perfectly re-dispersed in deionized water to prepare CNC suspensions at different accurate concentrations.

### Characterizations

#### Zetasizer

Malvern Instruments Zetasizer (ZEN 3600) was used to measure the electrophoretic mobility and size of CNC particles. Reported values are an average of 10 measurements.

#### Elemental analysis

The sulfur content (in weight percent) of different CNC samples have been measured by elemental analysis. The number of anionic sulfate half-ester groups ( $\text{SO}_3^-$ ) per 100 bulk anhydroglucose units has been found based on the formula of  $\text{C}_6\text{H}_{10}\text{O}_5-(\text{SO}_3)_n$  and calculated from the equation  $S(\text{wt}\%) = 100n \times S / [6C + 10H + (5 + 3n)O + nS]$ , as described in Hamad and Hu (2010).

#### Transmission electron microscopy

Transmission electron microscopy (TEM) images of the CNC crystallites were obtained using an FEI Tecnai G2 200 kV. To image the individual CNC crystallites, 1-mL drop of very dilute (~0.005 wt%) CNC suspension was deposited on a TEM grid immediately after sonication and dried under ambient condition. Image J software has been used to measure the physical dimensions of CNC particles.

#### Polarized optical microscopy

Photomicrographs of CNC suspensions were taken using a polarized light microscope (Mitutoyo microscope setup equipped with Lumenera LU 165 color CCD camera and polarizer). CNC suspensions were placed in the space between two glass plates of the rheometer (parallel plate geometry), and the microstructure was observed under crossed polarizer at 90°. The initial polarization is in flow direction, and the analyzer is perpendicular to flow. Images were taken during rheological testing and also at rest, during the drying process, close to the edges of the samples.

### Rheological measurements

The rheological measurements were performed using a rotational rheometer (MCR 502 Anton Paar Physica) equipped

**Table 1** Hydrolysis conditions for CNC suspensions used in the present work

Property Sample	Pulp Source	Pulp Consistency	Acid/Pulp (ml/g)	Reaction Temperature (°C)	Reaction Time (min)	Final Sample wt%	Yield (%)
CNC-A	BSKP	96.6	8.75	45	25	1.98	21
CNC-B	BSKP	96.4	6.00	45	25	3.80	32

**Table 2** Physicochemical characteristics of CNC suspensions examined in the current work

Property sample	Particle size (nm) (based on equivalent hydrodynamic volume measured by Zetasizer)	Electrophoretic mobility ( $\mu\text{m cm}/(\text{V s})$ )	Sulfur content (wt%)	OSO <sub>3</sub> H/100 anhydroglucose units
CNC-A	48.4	−1.377	0.85	4.39
CNC-B	46.0	−3.834	0.69	3.55

with a parallel plate glass geometry of 43 mm diameter. The steady-state shear viscosity versus shear rate curves were generated for all samples for shear rates in the range from 0.01 to 100 s<sup>−1</sup>. For each sample, the time required to reach steady state at 0.01 s<sup>−1</sup> was determined by a transient test; the sampling time used to generate the flow curves was decreased with increasing shear rate. Each data point in the viscosity versus shear rate curves is the average of three measurements. All steady shear data points are presented with error bars where the error bars are smaller than the size of the symbols in many cases.

Isothermal dynamic frequency sweeps were performed to determine the linear viscoelastic properties over the whole accessible frequency range. The strain amplitude used was 1–5 % during all small amplitude oscillation tests, where the samples have shown linear viscoelastic behavior determined by performing amplitude sweep experiments at a frequency of 1 Hz. To avoid evaporation, a small amount of silicone oil was placed on the periphery of samples together with an evaporation blocker. All rheological measurements were performed at the temperature of 25 °C.

#### Ultrasonic treatment (Sonication)

To disperse CNC particles, ultrasonic processor model VCX-130 (Sonics & Materials Inc.) with a 6-mm probe was used to apply ultrasound energy (in Joules per gram of CNC) to suspensions of different concentrations.

Ultrasonic treatment was carried out in an ice bath to avoid overheating, since the surface charge of CNC particles is heat-sensitive and an increase in temperature can cause de-esterification of the sulfate groups on the surface of the crystals (Beck-Candanedo et al. 2005).

## Results and discussion

### Characterization of CNC suspensions

During H<sub>2</sub>SO<sub>4</sub> hydrolysis, anionic sulfuric ester groups (SO<sub>3</sub><sup>−</sup>) are introduced on the surface of cellulose nanocrystals. Elemental analysis of the two sets of CNC suspensions under study yielded 0.85 and 0.69 wt% S, which leads to 4.39 and 3.55 OSO<sub>3</sub>H/100 anhydroglucose units for CNC-A and CNC-B, respectively (Table 2). Figure 1 shows TEM of these two samples. As can be seen in Fig. 1, the size and shape of the nanocrystals (being studied here) are practically the same for CNC suspensions with different degrees of sulfation, thereby allowing to independently examine the effects of surface charge on suspension rheology. The isolated nanocrystals were 7 ± 3 nm wide and 100 ± 8 nm long, giving an average aspect ratio in the range 10–20.

Both CNC-A and CNC-B suspensions formed chiral nematic liquid crystal structures above a critical concentration of 3 and 4 wt%, respectively. Representative polarized optical micrographs of 7 wt% CNC-A and CNC-B, with different degrees of sulfation, are shown in Fig. 2 in which the

**Fig. 1** TEM micrographs of samples **a** CNC-A and **b** CNC-B

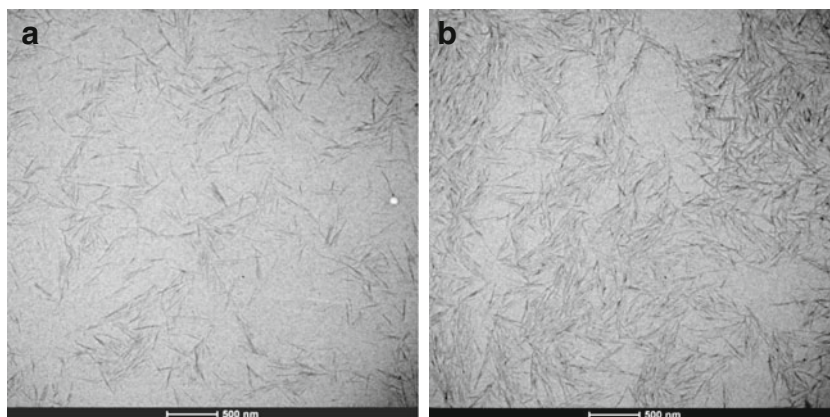
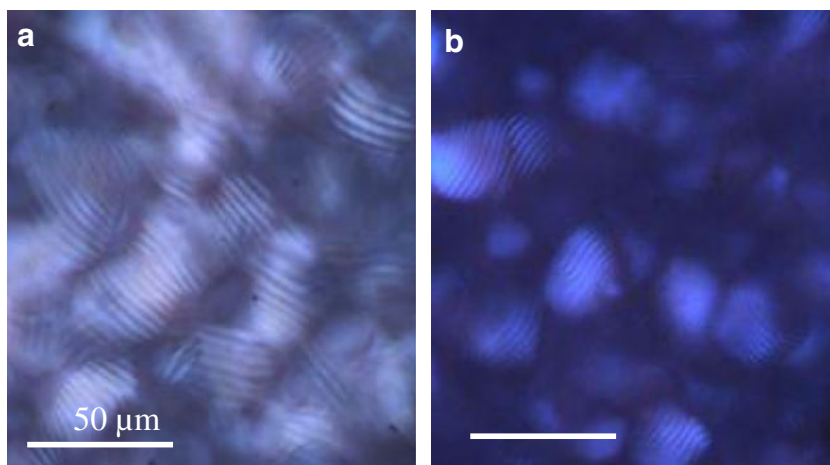


**Fig. 2** Polarized optical micrographs of 7 wt% **a** CNC-A and **b** CNC-B suspensions at 25 °C. Scale bars = 50  $\mu\text{m}$



fingerprint textures, characteristic of chiral nematic liquid crystals, clearly appear.

#### Viscosity of CNC suspensions

CNC suspensions at different concentrations were prepared from both CNC-A and CNC-B. To prepare well-dispersed CNC suspensions, ultrasound treatment (sonication) was used, which usually decreases the viscosity of suspensions (Marchessault et al. 1961; Dong et al. 1998; Shafiei-Sabet et al. 2012). We have previously studied the effect of sonication on viscosity of CNC suspensions systematically, showing that by increasing the amount of applied ultrasound energy (in joules per gram of CNC), the viscosity decreases. This decrease in viscosity is significant up to 1,000 J/g of CNC, due to breakage of aggregates in the system. By further increasing the applied sonication energy, the viscosity profile slightly changes with some changes occurring in the liquid crystalline structure. Similar experiments have also been performed in the current study for two different CNC suspensions, and the results are perfectly consistent with our previous findings (Shafiei-Sabet et al. 2012). Therefore, all the suspensions prepared for rheological testing in the current work are sonicated for 1,000 J/g of CNC, since it was previously concluded as a level of sonication sufficient to break most of the aggregates.

Figure 3 shows the steady-state viscosity curves for 5 wt% CNC-A (Fig. 3a) and CNC-B (Fig. 3b) suspensions before and after 1,000 J/g of CNC sonication. According to Fig. 3, decrease in the viscosity due to sonication is more pronounced in the case of CNC-B possessing a lower degree of sulfation. Lower surface charges cause a decrease in electrostatic repulsion (stability) of the nanoparticles, which leads to a higher probability of aggregation. Applied ultrasound energy breaks all these aggregates, and the viscosity then drops significantly.

The results of steady-state shear tests on the two different sets of CNC suspensions (CNC-A and CNC-B) at

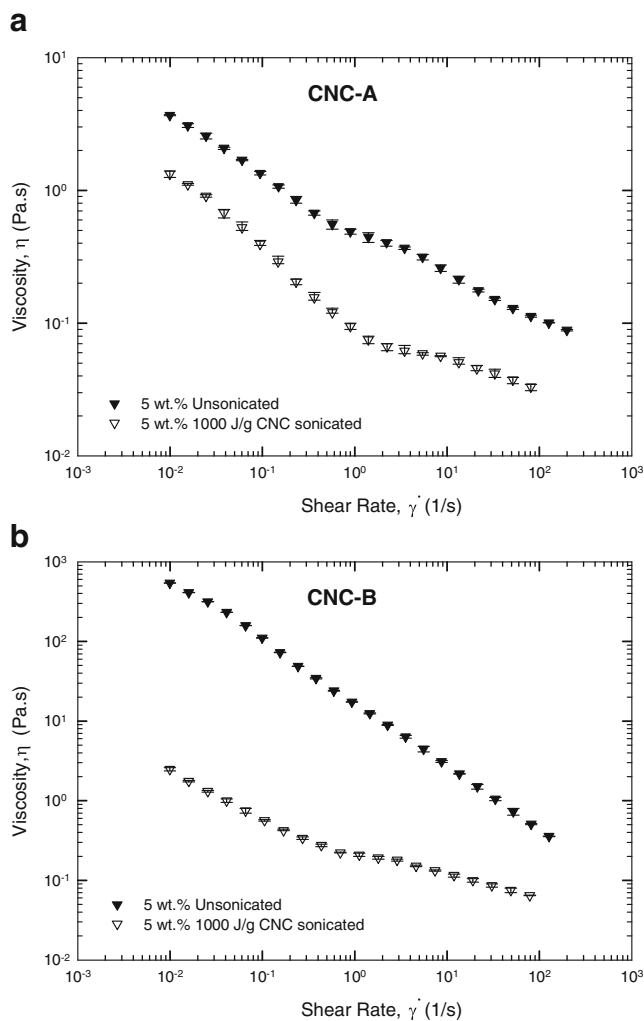


**Fig. 3** Effect of ultrasound energy on the viscosity material function of two different CNC suspensions, **a** CNC-A and **b** CNC-B

various concentrations ranging from 1 to 15 wt% are shown in Figs. 4 and 5, respectively. According to the viscosity profiles in these figures, by increasing the concentration, two transitions in rheological behavior were observed: (1) a transition from isotropic to liquid crystal and (2) a transition from liquid crystal to gel. For CNC-A suspensions (Fig. 4a, b), the 1 wt% CNC suspension behaves like an isotropic sample showing a Newtonian plateau at low shear rates, followed by shear-thinning at intermediate shear rates due to alignment of the nanorods in the shear direction, and another plateau at high shear rates where all the nanorods have been aligned—and therefore no further change in the viscosity occurs (Bercea and Navard 2000). By increasing the concentration above 3 wt%, liquid crystalline phases are formed in the suspension and the viscosity profile changes to the three-region profile, typical of liquid crystals (Onogi and Asada 1980). Figure 4a shows that this transition from

isotropic to anisotropic chiral nematic liquid crystal for CNC-A occurs at about 3 wt%, above which the viscosity profile consists of three different regions. Namely, (1) a shear-thinning region can be seen at low shear rates (due to alignment of chiral nematic liquid crystal domains), (2) a plateau at intermediate shear rates, where the domains have been all oriented along the shear direction, and (3) a second shear-thinning region at high shear rates, where the shear stress is high enough to destroy the liquid crystal domains and make it possible for individual nanorods to be oriented along the shear flow direction. This has been confirmed by neutron scattering (Orts et al. 1998) and polarized optical microscopy (Shafiei-Sabet et al. 2012).

By further increasing CNC concentration (Fig. 4b), the viscosity profile goes through another change from a three-region profile to one where a single shear-thinning behavior is observed over the whole range of investigated shear rates.

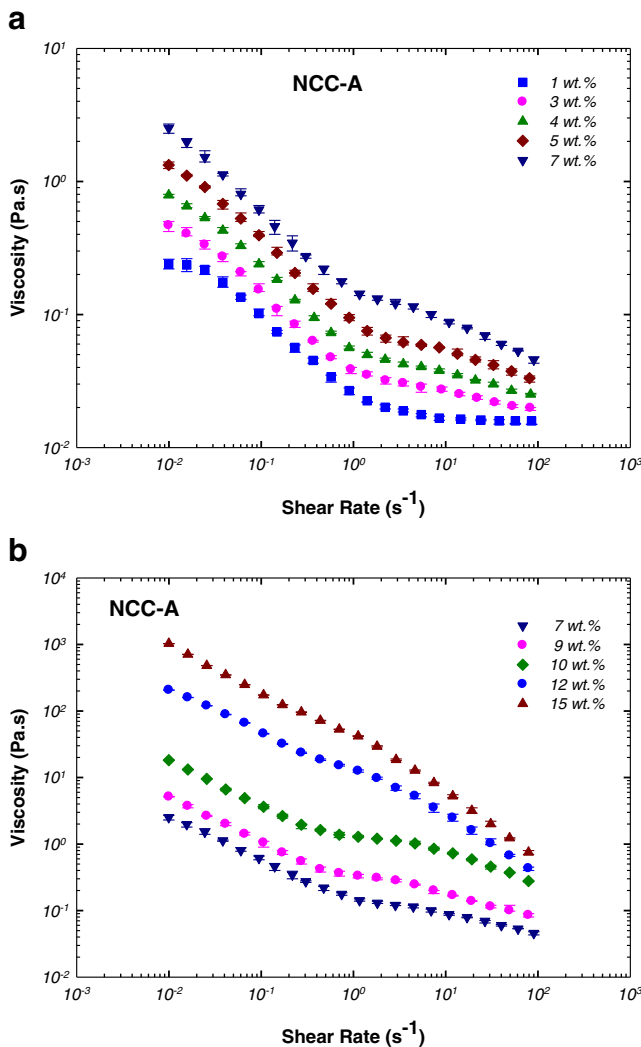


**Fig. 4** The viscosity material function of CNC-A suspensions, sonicated for 1,000 J/g of CNC, at concentrations of 1–7 wt% (a), and 7–15 wt% (b)

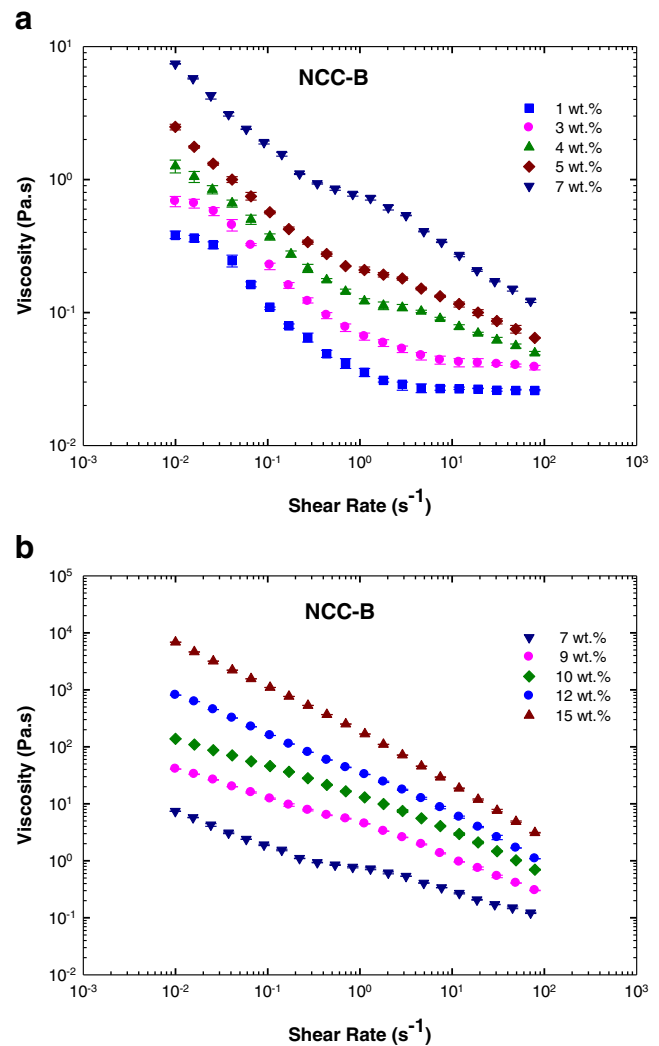


**Fig. 5** The viscosity material function of CNC-B suspensions, 1,000 J/g of CNC, at concentrations of 1–7 wt% (a) and 7–15 wt% (b)

This change can be attributed to another transition from liquid crystal to gel-like structure (Urena-Benavides et al. 2011; Liu et al. 2011; Shafiei-Sabet et al. 2012), where gel formation inhibits the formation of chiral nematic ordered phases. According to Fig. 4b, this transition occurs at about 12 wt% for CNC-A, the suspension possessing high surface charge. More evidence to the gel formation will be presented below, in Section “[Linear viscoelastic measurements \(gel formation\)](#).”

For CNC-B, the suspension with a lower degree of sulfation, rheological measurements (Fig. 5a) reveal that the transition from isotropic to anisotropic and the formation of chiral nematic liquid crystals occur at about 4 wt%, above which the three-region viscosity curves often observed in liquid crystalline CNC suspensions become evident. By further increasing CNC concentration, the suspension shows a tendency to form a gel and goes through a second transition, liquid crystal to gel, at about 10 wt% (relatively at a lower concentration compared with CNC-A). This transition is more clearly shown below where the linear viscoelastic moduli of various suspensions are presented.

The tendency of CNC-B suspensions to form gel apparently inhibits the formation of chiral nematic liquid crystal

phases at concentrations where they are readily observed for the CNC-A nanocrystals. These results are consistent with studies by Araki et al. (1998, 1999), who also reported changes in viscosity behavior of cellulose nanocrystals prepared by different methods. More studies are yet needed to fully understand the factors governing the relative tendencies of CNC particles to gel rather than form ordered phases. However, knowing that the dimensions and shape of CNC particles in these two sets of CNC samples are equal (see Fig. 1), it can be concluded that lower degree of sulfation, which leads to lower electrostatic repulsion, is the main parameter contributing to gel formation (gelation process).

To follow changes in the structure of these suspensions under shear, polarized optical microscopy has been used online, coupled with a rheometer, to capture in situ polarized optical microscopy (POM) micrographs at various shear rates. Typical micrographs of 9 wt% CNC-A suspension (a liquid crystalline sample) and a 12 wt% CNC-A suspension (a gel) are shown in Figs. 6 and 7, respectively. For 9 wt% CNC-A sample (Fig. 6), the sample shows fingerprint texture characteristic of chiral nematic ordered domains at rest (Fig. 6a), and the suspension goes through three distinct microstructural changes under shear. The POM micrographs

**Fig. 6** Polarized optical micrographs of 9 wt% CNC-A suspensions at rest (**a**) and during steady shear tests at shear rates of **b**  $0.01 \text{ s}^{-1}$ , **c**  $0.1 \text{ s}^{-1}$ , **d**  $0.5 \text{ s}^{-1}$ , **e**  $1 \text{ s}^{-1}$ , and **f**  $10 \text{ s}^{-1}$

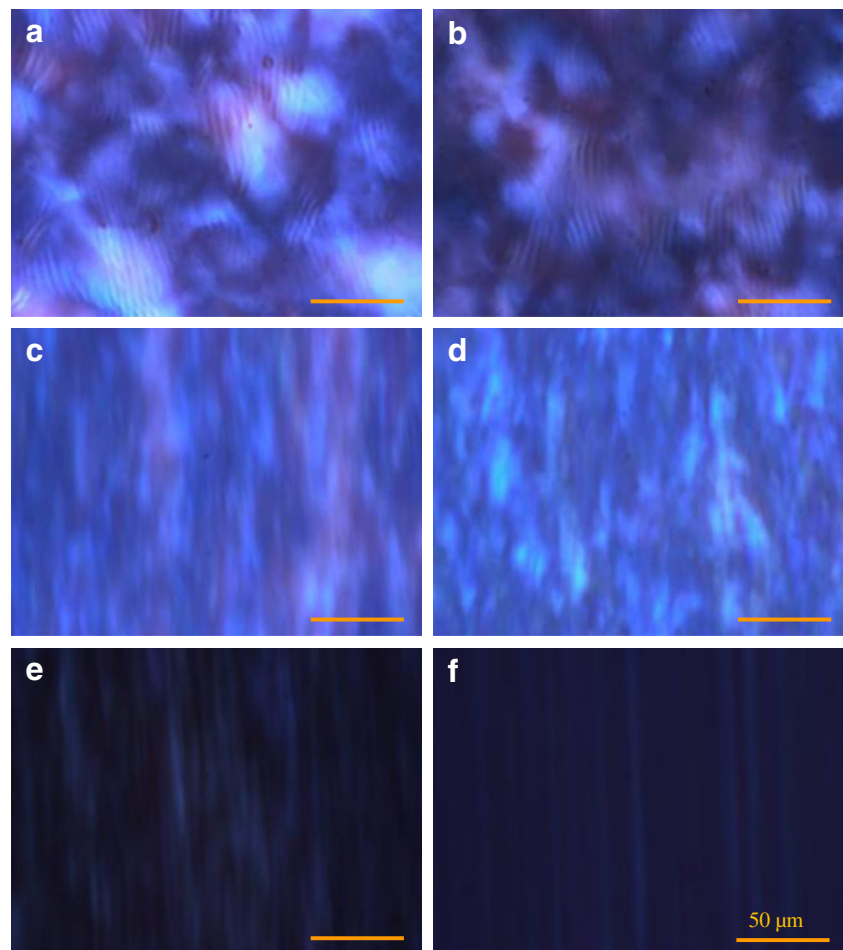
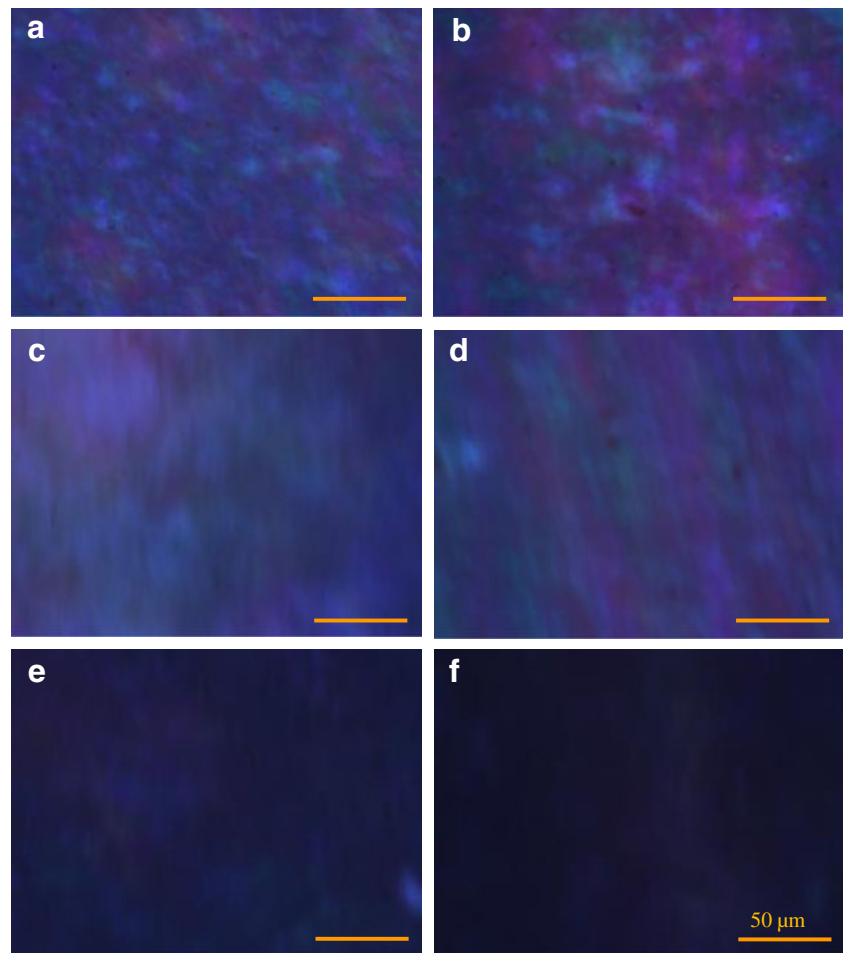


**Fig. 7** Polarized optical micrographs of 12 wt% CNC-A suspensions at rest (**a**) and during steady shear tests at shear rates of **b**  $0.01\text{ s}^{-1}$ , **c**  $0.1\text{ s}^{-1}$ , **d**  $0.5\text{ s}^{-1}$ , **e**  $1\text{ s}^{-1}$ , **f**  $10\text{ s}^{-1}$



of Fig. 6b–d represent the first shear-thinning region, where viscosity decreases due to deformation and re-alignment of chiral nematic domains. In the plateau region, these domains become aligned along the shear direction (Fig. 6e), and eventually break down (hence, the micrograph appears black). This last dark micrograph (Fig. 6f) indicates that the liquid crystal domains are broken and are no longer present in the suspension at higher shear rates. The individual CNC rods essentially align themselves in this shear rate region (typically higher than  $10\text{ s}^{-1}$ ).

For the 12 wt% CNC-A sample (Fig. 7), the sample is a birefringent gel at rest (Fig. 7a) and the gel structure breaks under shear but remains birefringent up to shear rate of  $1\text{ s}^{-1}$ .

#### *Morphology of the CNC suspensions during shear*

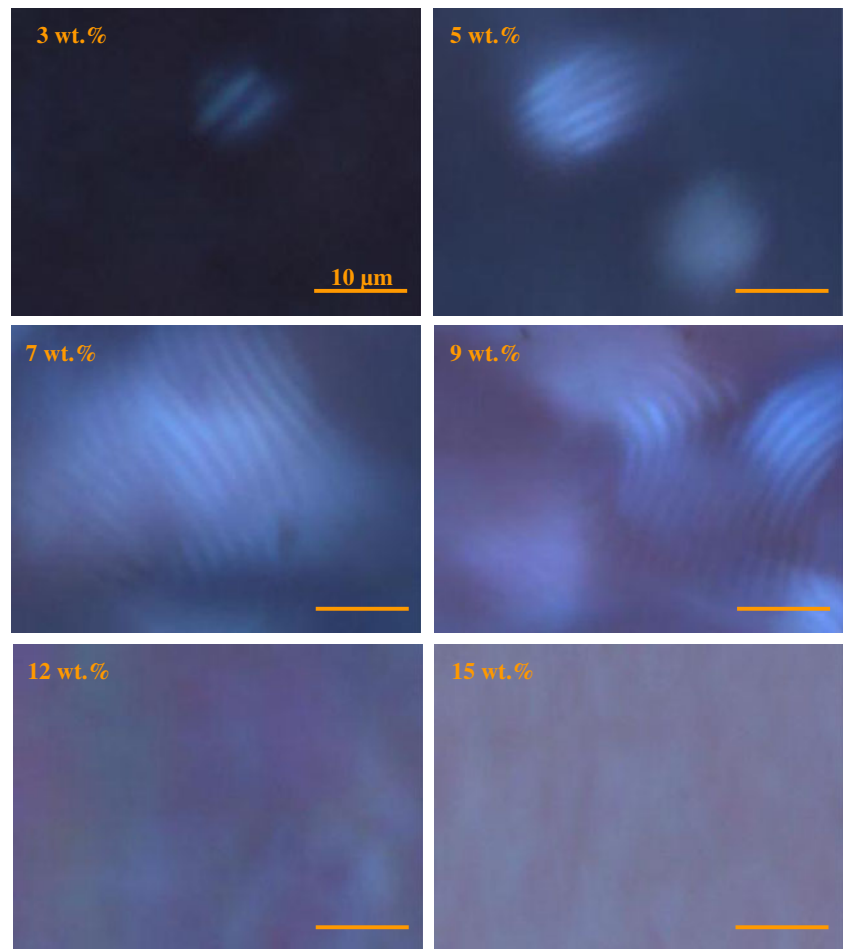
Polarized optical microscopy has been used online with a rotational rheometer to capture micrographs of samples at different concentrations in order to follow phase transitions. Figure 8 shows the micrographs of CNC-A suspensions at different concentrations and at shear rate of  $0.01\text{ s}^{-1}$ . At 3 wt%, the micrograph shows the existence of small

domains of liquid crystalline structure (fingerprint texture) in a biphasic region. By increasing the concentration up to 7 wt%, the fraction of liquid crystal domains in the biphasic system increases. At 9 wt%, the liquid crystalline structure appears in the entire micrograph and the fingerprint texture, which is characteristic of cholesteric liquid crystals, can be seen all across the sample. Further increase in CNC concentration results in birefringent gels and no fingerprint can be observed in the POM micrographs of suspensions with concentrations above 12 wt%.

For CNC-B (Fig. 9) at 3 wt%, the micrograph appeared black, indicating no liquid crystal ordered phases at this concentration. The fingerprint patterns begin to appear at 5 wt%, and disappear at 10 wt% where the micrograph shows a birefringent gel structure—a random structure with bright colors. Rheological characterization of these samples also confirms the occurrence of gel formation in CNC-B suspensions.

In the case of CNC-B, a lower degree of sulfation results in decreased intermolecular interactions which further results in gel phase formation at a lower concentration. On the other hand, the higher surface charge in CNC-A favors the formation of anisotropic liquid crystalline phases.

**Fig. 8** Polarized optical micrographs of CNC-A suspensions at different concentrations, taken at shear rate of  $0.01 \text{ s}^{-1}$ . The scale bar is  $10 \mu\text{m}$



Due to repulsive particle interactions, a lower concentration of CNC particles is enough to frustrate packing in random orientation and transition from isotropic to anisotropic occurs.

#### *Linear viscoelastic measurements (gel formation)*

To carefully examine gel transition in high-concentration CNC suspensions, isothermal frequency sweep tests were performed to measure the linear viscoelastic moduli. Namely, the storage modulus  $G'$ , and loss modulus  $G''$  of CNC-A and CNC-B suspensions having various concentrations are shown in Figs. 10 and 11, respectively. Only a few concentrations are shown for the sake of clarity. For CNC-A suspensions, samples with concentrations of 10 wt% and lower behaved as predominantly viscous fluids (loss modulus,  $G''$ , being higher than storage modulus,  $G'$ , over the whole investigated frequency range). For the 12 wt% sample, a gel-like behavior was observed, where  $G'$  and  $G''$  overlap over an extended range of frequency. At 15 wt% concentration, the behavior resembles that of a viscoelastic solid, where the  $G'$  is independent of frequency and higher than  $G''$  over the entire investigated frequency range,

indicating formation of a stiff gel. The three different behaviors, liquid-like, gel, and solid-like, can be seen for 10, 12, and 15 wt% CNC-A, respectively.

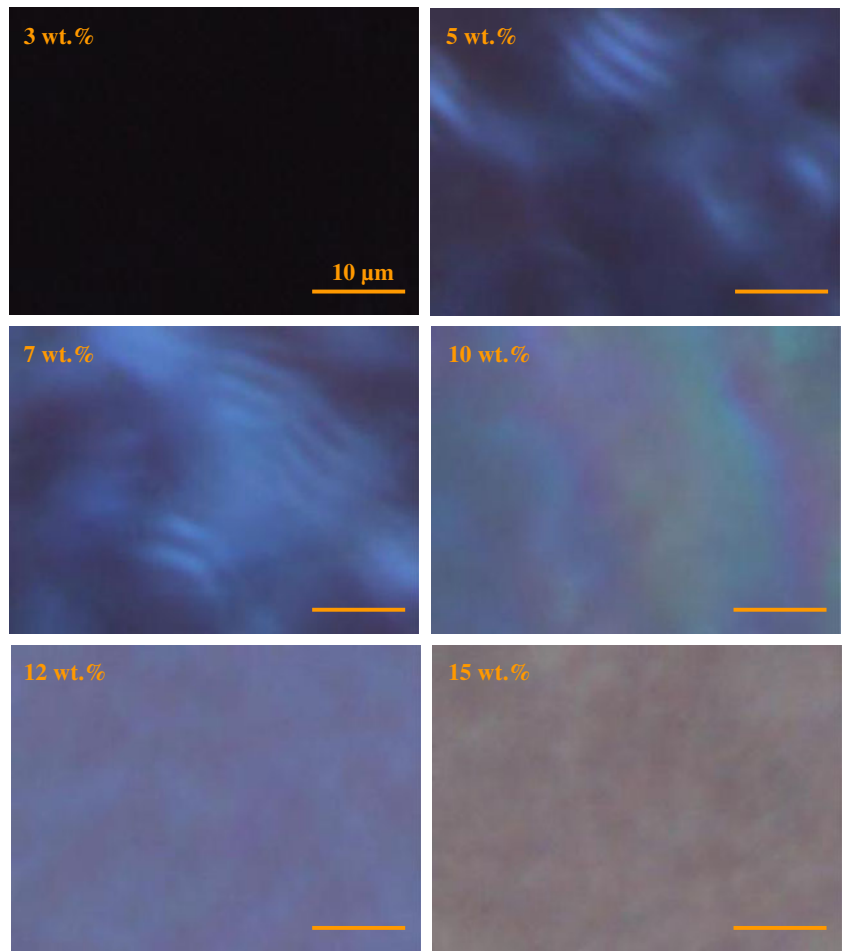
Based on the rheological data presented in Fig. 10 for CNC-A suspensions having a higher degree of sulfation, and at the temperature used for rheological measurements ( $25 \text{ }^\circ\text{C}$ ), the transition from liquid crystalline to gel occurs at about 12 wt%. These results are supported by the POM micrographs presented in Fig. 8, which have clearly shown the disappearance of fingerprint texture upon transition from liquid crystalline into a gel phase. For CNC-B suspensions (Fig. 11), the suspension possessing a lower degree of sulfation, gel formation happens at the lower concentration of 10 wt%, consistent with the optical microscopy results presented in Fig. 9.

#### *The Cox–Merz rule*

One of the common rheological characteristics of lyotropic liquid crystals and gels is that the Cox–Merz rule is not obeyed, which means the steady-state viscosity  $|\eta(\gamma)|$  and complex viscosity  $|\eta^*(\omega)|$  are not equal when compared at the same shear rate  $\gamma$  and frequency  $\omega$  (Davis et al.



**Fig. 9** Polarized optical micrographs of CNC-B suspensions at different concentrations, taken at shear rate of  $0.01 \text{ s}^{-1}$ . The scale bar is  $10 \mu\text{m}$



2004; Urena-Benavides et al. 2011; Shafiei-Sabet et al. 2012). This is also the case for many other systems that exhibit structural formation that is preserved under linear viscoelastic measurements (complex viscosity) and breaks

down under shear (absolute viscosity)—such as in concentrated pulp suspensions (Doraiswamy et al. 1991), in soft solids such as dough and mozzarella (Muliawan and Hatzikiriakos 2007; Sofou et al. 2008), and in exfoliated

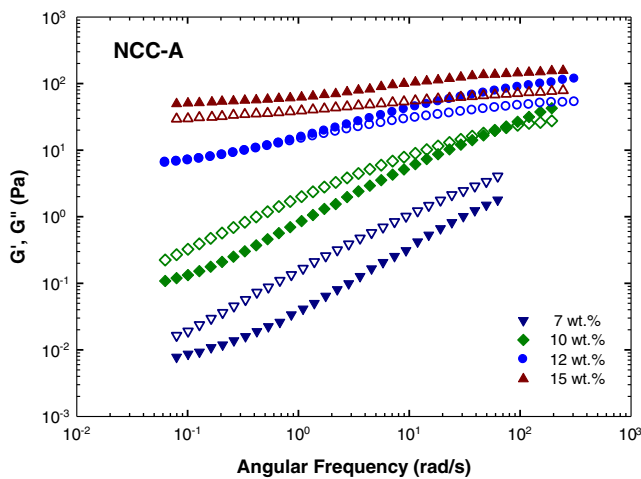


**Fig. 10** Storage modulus,  $G'$  (solid symbols), and loss modulus,  $G''$  (open symbols), versus angular frequency,  $\omega$ , for CNC-A suspensions sonicated for 1,000 J/g CNC and at different concentrations

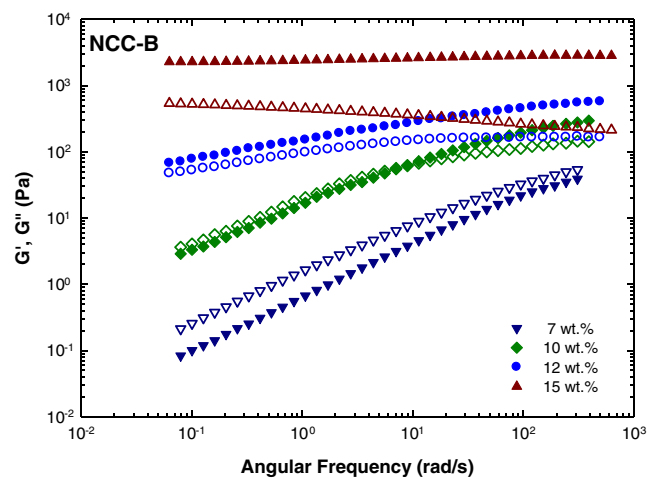


**Fig. 11** Storage modulus,  $G'$  (solid symbols), and loss modulus,  $G''$  (open symbols), versus angular frequency,  $\omega$ , for CNC-B suspensions sonicated for 1,000 J/g CNC and at different concentrations

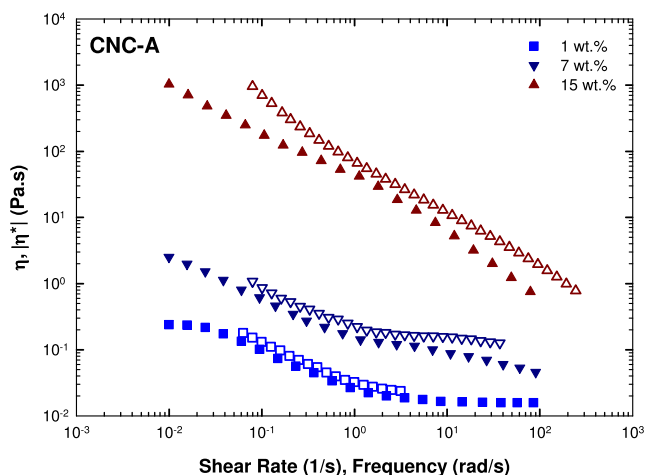


**Fig. 12** Cox–Merz plot for CNC-A suspensions at different concentrations (sonicated at 1,000 J/g of CNC). All the concentrations of 1–15 wt% have been tested, but results only for 1, 7, and 15 wt% are presented in this figure for the sake of clarity. *Solid symbols* are shear viscosities and *open symbols* are complex viscosities. Failure of Cox–Merz indicates significant structural formation

polymer nanocomposites (Devendra et al. 2006). To study the applicability of the Cox–Merz rule, the complex and shear viscosities of CNC-A and CNC-B suspensions at different concentrations (sonicated at 1,000 J/g CNC) were compared and plotted in Figs. 12 and 13, respectively. For CNC-A (Fig. 12), the 1 wt% isotropic sample obeys the Cox–Merz. By increasing CNC concentration and formation of chiral nematic ordered domains, the behavior deviates from the Cox–Merz rule and the deviation becomes more significant with further increase in concentration. In

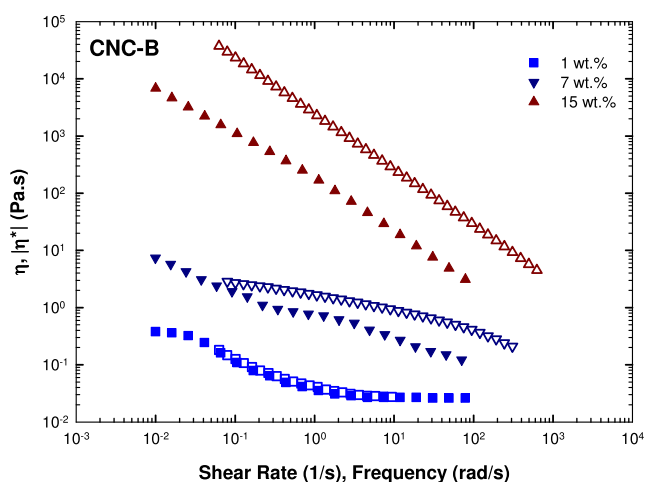


**Fig. 13** Cox–Merz plot for CNC-B suspensions at different concentrations (sonicated at 1,000 J/g of CNC). All the concentrations of 1–15 wt% have been tested, but results only for 1, 7, and 15 wt% are presented in this figure for the sake of clarity. *Solid symbols* are shear viscosities and *open symbols* are complex viscosities

the case of CNC-B samples (Fig. 13), Cox–Merz applies up to 3 wt% (isotropic samples), thereby confirming there is minimal structural formation at this level of concentration, which is in agreement with the results from polarized light microscopy (Fig. 9). At concentrations above 4 wt%, all the samples deviate, especially at higher shear rates (or frequency). A further increase in concentration, and going through gellation, lead to significant deviation from Cox–Merz throughout the entire shear rate (or frequency) range. Shear flow breaks the gel and affects the structure, and therefore, the dynamic low strain data do not follow the steady-state shear data. The Winter plots (Winter 2009) were also plotted for all samples (not included in this paper) which confirmed the deviation of these suspensions from Cox–Merz rule.

## Conclusions

Two different sets of cellulose nanocrystal suspensions, possessing different degrees of sulfation, were prepared by  $H_2SO_4$  acid hydrolysis of black spruce kraft pulp. The CNC suspensions exhibit isotropic to chiral nematic liquid crystalline phase transition above a first critical concentration, where the fingerprint texture, characteristic of cholesteric liquid crystals, can be observed under polarized optical microscopy. Biphasic and liquid crystalline samples show a three-region viscosity behavior, as expected for lyotropic polymer liquid crystals. It was found that, by further increasing concentration, the CNC suspension goes through another transition, liquid crystal to gel, above a second critical concentration.

The rheological properties and microstructure of these CNC suspensions have been systematically studied over a wide concentration range of 1 to 15 wt% to capture both transitions in microstructure. It was found that the degree of sulfation of CNC particles significantly affects the critical concentrations for those transitions to occur. Gel formation has been studied by dynamic frequency sweep tests at the linear viscoelastic region, in order to determine the critical concentration for gel formation at which  $G'$  and  $G''$  overlap over an extended range of frequency. Above this second critical concentration, CNC suspensions showed solid-like behavior, where  $G'$  was independent of frequency and higher than  $G''$  over the entire evaluated frequency range. Furthermore, no fingerprint texture was present in the POM micrographs of these high-concentration samples. The applicability of the Cox–Merz rule has been studied for the two different CNC suspensions at different concentrations. It has been shown that CNC suspensions violate this rule for concentrations greater than a critical value indicating significant structural formation, in agreement with polarized microscopy analysis.

**Acknowledgments** The authors would like to acknowledge NSERC and FPInnovations for financial support under grant CRD-379851-2008.

## References

- Araki J, Wada M, Kuga S, Okano T (1998) Flow properties of microcrystalline cellulose suspension prepared by acid treatment of native cellulose. *Colloids Surf A Physicochem Eng Asp* 142(1):75–82
- Araki J, Wada M, Kuga SH, Okano T (1999) Influence of surface charge on viscosity behavior of cellulose microcrystal suspension. *J Wood Sci* 45:258–261
- Beck-Candanedo S, Roman M, Gray DG (2005) Effect of reaction conditions on the properties and behavior of wood cellulose nanocrystal suspensions. *Biomacromolecules* 6:1048–1054
- Bercea M, Navard P (2000) Shear dynamics of aqueous suspensions of cellulose whiskers. *Macromolecules* 33:6011–6016
- Boluk Y, Lahiji R, Zhao L, McDermott MT (2011) Suspension viscosities and shape parameter of cellulose nanocrystals (CNC). *Colloids Surf A Physicochem Eng Asp* 377:297–303
- Davis VA, Ericson LM, Parra-Vasquez ANG, Fan H, Wang Y, Prieto V, Longoria JA, Ramesh S, Saini RK, Kittrell C, Billups WE, Adams WW, Hauge RH, Smalley RE, Pasquali M (2004) Phase behavior and rheology of SWNTs in superacids. *Macromolecules* 37:154–160
- Devendra R, Hatzikiriakos SG, Vogel R (2006) Rheology of metallocene polyethylene based nanocomposites: influence of graft modification. *J Rheol* 50:415–434
- Dong XM, Kimura T, Revol JF, Gray DG (1996) Effects of ionic strength on the isotropic-chiral nematic phase transition of suspensions of cellulose crystallites. *Langmuir* 12(8):2076–2082
- Dong XM, Revol JF, Gray DG (1998) Effect of microcrystallite preparation conditions on the formation of colloid crystals of cellulose. *Cellulose* 5:19–32
- Doraiswamy D, Mujumdar AN, Tsao I, Beris AN, Danforth SC, Metzner AB (1991) The Cox–Merz rule extended—a rheological model for concentrated suspensions and other materials with a yield stress. *J Rheol* 35(4):647–685
- Hamad WY, Hu TQ (2010) Structure–process–yield interrelation in nanocrystalline cellulose extraction. *Can J Chem* 88(3):392–402
- Kang K, Lettinga MP, Dogic Z, Dhont JKG (2006) Vorticity banding in rodlike virus suspensions. *Phys Rev E* 74:026307–1–12
- Lettinga MP, Dogic Z, Wang H, Vermant J (2005) Flow behavior of colloidal rodlike viruses in the nematic phase. *Langmuir* 21:8048–8057
- Liu D, Chen X, Yue Y, Chen M, Wu Q (2011) Structure and rheology of nanocrystalline cellulose, carbohydrate. *Polymer* 84:316–322
- Marchessault RH, Morehead FF, Walter NM (1959) Liquid crystal systems from fibrillar polysaccharides. *Nature* 184:632–633
- Marchessault RH, Morehead FF, Koch MJ (1961) Some hydrodynamic properties of neutral suspensions of cellulose crystallites as related to size and shape. *J Colloid Sci* 16:327–344
- Muliawan EB, Hatzikiriakos SG (2007) Rheology of mozzarella cheese. *Intern Dairy J* 17:1063–1072
- Odijk T (1986) Theory of lyotropic liquid crystals. *Macromolecules* 19:2313–2329
- Onogi S, Asada T (1980) In rheology and rheo-optics of polymer liquid crystals. In: Astarita G, Marrucci G, Nicolais L (eds) *Proceedings of the eighth international congress on rheology*. Plenum, Naples, pp 126–136
- Onsager L (1949) The effect of shape on the interactions of colloid particles. *Ann N Y Acad Sci* 51:627–659
- Orts WJ, Godbout L, Marchessault RH, Revol JF (1998) Enhanced ordering of liquid crystalline suspensions of cellulose microfibrils: a small angle neutron scattering study. *Macromolecules* 31:5717–5725
- Revol JF, Marchessault RH (1994) In vitro chiral nematic ordering of chitin crystallites. *Int J Biol Macromol* 15:329–335
- Revol J, Bradford H, Giasson J, Marchessault RH, Gray DG (1992) Helicoidal self-ordering of cellulose microfibrils in aqueous suspension. *Int J Biol Macromol* 14(3):170–172
- Ripoll M, Holmqvist P, Winkler RG, Gompper G, Dhont JKG, Lettinga MP (2008) Attractive colloidal rods in shear flow. *Phys Rev Lett* 101:168302–1–4
- Shafiei-Sabet S, Hamad WY, Hatzikiriakos SG (2012) Rheology of nanocrystalline cellulose aqueous suspensions. *Langmuir* 28:17124–17133
- Sofou S, Muliawan EB, Hatzikiriakos SG, Mitsoulis E (2008) Rheological characterization and constitutive modelling of bread dough. *Rheol Acta* 47:369–381
- Urena-Benavides EE, Ao G, Davis VA, Kitchens CL (2011) Rheology and phase behavior of lyotropic cellulose nanocrystal suspensions. *Macromolecules* 44:8990–8998
- Winter HH (2009) Three view of viscoelasticity for Cox–Merz materials. *Rheol Acta* 48:241–243